ELSEVIER

Catalysis Today 62 (2000) 189–199

CATALYSIS TODAY

www.elsevier.com/locate/cattod

Oxidative catalytic removal of hydrocarbons over Pt/Al_2O_3 catalysts

T.F. Garetto, C.R. Apesteguía*

Instituto de Investigaciones en Catálisis y Petroquímica-INCAPE (UNL-CONICET) Santiago del Estero 2654, 3000 Santa Fe, Argentina

Abstract

The reaction kinetics, structure sensitivity, and in situ activation of cyclopentane and methane combustions were studied on Pt/Al_2O_3 catalysts of different platinum and chlorine loadings. The catalyst activities were evaluated through both conversion vs. temperature (light-off curves) and conversion vs. time catalytic tests. Cyclopentane oxidation turnover rates (TOF) increased dramatically with increasing Pt crystallite size while TOF values for methane oxidation increased only three times by diminishing the Pt dispersion from 65 to 15%. The reaction orders in oxygen were one (cyclopentane) and zero (CH_4). For both reactions, the orders and activation energies did not change by changing the Pt dispersion. Results are interpreted in basis of two different reaction mechanisms over the metallic Pt active sites. Cyclopentane oxidation proceeds via a surface redox mechanism, being the dissociative adsorption of oxygen the rate-determining step. The observed turnover rate increase with increasing Pt particle size reflects an increase in the density of reactive Pt–O species resulting from higher Pt oxidation rates. The methane oxidation mechanism is interpreted in terms of Mars–van Kravelen reduction–oxidation pathways which include the abstraction of the first hydrogen on the adsorbed methane molecule as the rate-determining step. Low-conversion catalytic tests performed at constant temperature showed that on well-dispersed Pt/Al_2O_3 catalysts the cyclopentane conversion increases with time on stream, while the methane activity decreases. Activating induction periods during the oxidation of cyclopentane are related to the sintering of the metallic phase in reaction conditions. Hot-spots on the metallic particles together with the presence of gaseous water cause the formation of larger, more reactive, Pt crystallites, even at mild reaction conditions. The activation phenomenon ab initio of the reaction is not verified for methane oxidation on Pt/Al_2O_3 catalysts. The different structure sensitivity of the slowest steps in the reaction–oxidation mechanisms explains the existence of induction periods on well-dispersed Pt catalysts only for cyclopentane oxidation.

Keywords: Hydrocarbon combustion; Pt/Al_2O_3 catalysts; Methane oxidation mechanism; Cyclopentane oxidation mechanism

1. Introduction

Platinum supported on alumina carriers are widely employed for the combustion of non-halogenated volatile organic compounds (VOCs) [1–3]. Particularly, platinum-based catalysts are highly active for oxidative removal of small amounts of hydrocarbon from gaseous or liquid streams; excepting for palladium in the case of methane, platinum is recognized to be the most active metal for hydrocarbon oxidation [4,5]. The effect of varying the platinum particle size on the catalytic combustion of different hydrocarbons has been extensively studied [6–15], but the results obtained are conflicting, probably because correlation between catalytic activity and metallic dispersion depends on the type of hydrocarbon to be abated. Several papers on light alkanes and aromatics combustion, namely methane [6–8], propane [15], butane

* Corresponding author. Tel.: +54-342-4555279; fax: +54-342-4531068.
E-mail address: capesteg@fiqus.unl.edu.ar (C.R. Apesteguía).

0920-5861/00/$ – see front matter
PII: S0920-5861(00)00420-X

[9], heptane [10] and benzene [14] have reported that oxidation turnover rates increase with increasing platinum particle size. In contrast, in a recent study on the C_2H_4 combustion over platinum-supported catalysts Pliangos et al. [16] proposed that turnover frequency changes, which cannot be explained by structure sensitivity considerations, are caused by interactions between the metal crystallites and the carrier. Papaefthimiou et al. [17] reported that the benzene oxidation turnover rate on Pt/Al_2O_3 strongly increases with increasing Pt particle size but does not change by changing the Pt dispersion on Pt/SiO_2 and Pt/TiO_2 catalysts.

Platinum catalysts are often activated on stream, ab initio of the hydrocarbon combustion reaction. The existence of induction periods during the deep oxidation of hydrocarbons has also been reported on palladium-based catalysts; in the case of methane oxidation, several authors have proposed that the initial activation period is caused by reoxidation from Pd metal or oxygen-deficient PdO_x to more active steady state PdO species [18,19]. In contrast, very few papers have been published using platinum-based catalysts and the causes of induction periods on platinum remain unclear. A similar explanation than that proposed above for Pd catalysts is unlikely because there is a general agreement that hydrocarbon oxidation reactions over platinum occur on metallic sites [20]. Marceau et al. [21] observed that on chlorided Pt/Al_2O_3 catalysts the activity for methane oxidation increases with time concomitantly with chlorine elimination from the support. They concluded that the initial catalyst activation is caused by the elimination of chlorine on stream which increases the accessibility of reactant gases to the active metallic Pt sites. However, we recently found [14] that the existence of induction periods during benzene oxidation on Pt/Al_2O_3 is not caused by the presence of chlorided ions on the catalyst but by the sintering of Pt crystallites in reaction conditions.

In this work we have extended the above studies to include results on the oxidation of cyclopentane and methane over a set of Pt/Al_2O_3 catalysts of different metallic dispersion and chlorine concentration. Our goal was to obtain further information on the catalyst activation phenomenon and on the sensitivity of hydrocarbon oxidation turnover rates to Pt crystallite size.

2. Experimental

2.1. Catalyst preparation and characterization

A chlorided $Pt(0.26\%)/Al_2O_3$ catalyst (catalyst A-I) was prepared by impregnation at 303 K of a high-purity γ-Al_2O_3 powder (Cyanamid Ketjen CK300) with an aqueous solution of chloroplatinic acid, $H_2PtCl_6{\cdot}6H_2O$ (Aldrich, 99.995%) and HCl. The CK300 alumina has BET surface area of 180 m^2/g, pore volume of 0.49 cm^3/g and contains 50 ppm sulfur. After impregnation, the sample was dried for 12 h at 393 K and heated in air stream to 773 K. Then the chlorine content was regulated using a gaseous mixture of HCl, water and air. Finally, the sample was purged with N_2 and reduced in flowing H_2 for 4 h at 773 K. Two catalysts with different Pt dispersions were prepared by treating two portions of catalyst A-I in a 2% O_2/N_2 atmosphere for 2 h at 848 and 903 K, respectively, and then reduced for 4 h at 773 K; the resulting sintered catalysts are identified here as catalysts A-II and A-III, respectively. A chlorine-free $Pt(0.38\%)/Al_2O_3$ catalyst (catalyst B-I) was prepared by impregnation at 303 K of CK300 alumina with an aqueous solution of tetraamine platinum nitrate, $Pt(NH_3)_4(NO_3)_2$ (Alfa) for 6 h. The impregnated alumina was dried overnight at 393 K, then heated in air at 773 K for 4 h and finally reduced for 4 h at 773 K in hydrogen. A portion of catalyst B-I was treated for 2 h in a 2% O_2/N_2 mixture at 858 K in order to sinter the metallic fraction and then reduced for 4 h at 773 K (catalyst B-II). The main characteristics of the samples are shown in Table 1.

The platinum dispersion (D) was determined by irreversible H_2 chemisorption. The volumetric adsorption experiments were performed at 298 K in a conventional vacuum instrument equipped with an MKS Baratron pressure gauge. The double isotherm method was used [22]: the first isotherm gave the total gas uptake and the second, obtained after 1 h of evacuation at room temperature, the weakly adsorbed gas. By difference, the amount of irreversibly held H_2, $(HC)_i$, was calculated as the difference between total and weakly adsorbed H_2. The pressure range of isotherms was 0–0.35 atm (1 atm = 101.3 kPa) and extrapolation to zero pressure was used as a measure of the gas uptake on the metal. A stoichiometric atomic ratio $(HC)_i/Pt_s = 1$, where Pt_s implies a Pt

Table 1
Characteristics of the catalysts used in this work

Catalyst	Pt loading (wt.%)	Pt dispersion D_0 (%)	Surface Pt concentration (μmol Pt_s/g catalyst)	Mean Pt particle size $\bar{d}_{Pt}$ (Å)	Chlorine concentration (wt.%)
A-I	0.26	65	8.7	13	0.95
A-II	0.26	38	5.1	22	0.61
A-III	0.26	15	2.0	57	0.58
B-I	0.38	55	10.7	15	0
B-II	0.38	19	3.7	45	0

atom on surface, was used to calculate the platinum dispersion. Catalysts were outgassed at 773 K in a vacuum of 8×10^{-8} atm and then reduced in H_2 at 573 or 773 K for 2 h prior to performing gas chemisorption experiments. Mean Pt crystallite sizes ($\bar{d}_{Pt}$, Å) were determined from H_2 chemisorption data by using site densities of 1.12×10^{15} sites per cm^2 of metal [23].

Platinum loadings were measured by atomic absorption spectrometry, whereas chlorine contents on the catalysts were determined by chemical analysis, using conventional colorimetric techniques.

2.2. Catalytic tests

Hydrocarbon oxidation reactions were carried out at 1 atm in a fixed-bed tubular reactor (Pyrex, 0.8 cm ID). Catalyst samples were held as a thin layer above a plug of acid-washed quartz wool. Temperatures were measured using a K type thermocouple placed into the catalyst bed. Samples were sieved and fraction 0.35–0.42 mm was separated and loaded to the reactor. In standard runs, catalyst loadings (W) of 0.4 g and contact times (W/F^0) of 54 g catalyst h/mol cyclopentane and of 20 g catalyst h/mol methane were used. Cyclopentane (Fluka, purity >99%) or methane (Air Liquide, 99.5%) were fed in concentrations of 0.65 and 2%, respectively, in a 10% O_2/N_2 mixture. On-line chromatographic analysis was performed using a gas chromatograph Shimadzu GC-8A equipped with a flame ionization detector and Bentone 34 or Porapak Q packed columns. Before gas chromatographic analysis, the reaction products were separated and carbon dioxide converted to methane by means of a methanation catalyst (Ni/Kieselghur) operating at 673 K. The presence of water in the products was verified but not quantified. Carbon monoxide was never detected in the effluent. Before catalytic measurements, all the catalysts were reduced in hydrogen at 673 K for 1 h and then cooled to the desired temperature. Two experimental procedures were used for catalyst testing. The complete oxidation of hydrocarbons was studied by obtaining curves of hydrocarbon conversion (X) as a function of temperature (light-off curves). The temperature was raised by steps of about 23 K, from 373 to 673 K (cyclopentane) or 913 K (methane). More fundamental differential reactor experiments (less than 10% conversion) were performed at constant temperature. The products were sampled at 5 min intervals using an automated sampling valve. In steady-state rate measurements, diffusional limitations were ruled out by varying particle sizes and contact times between 0.15 and 0.49 mm and 5 and 200 g catalyst h/mol hydrocarbon, respectively.

3. Results

3.1. Catalytic tests: light-off curves

Fig. 1 shows the X vs. T curves obtained for cyclopentane and methane combustion on catalysts A-I, A-II and A-III. On catalyst A-I, the cyclopentane oxidation starts at about 473 K and the conversion increases then dramatically at ca. 553 K reaching a value of $X \cong 100\%$ between 653 and 673 K. The light-off curves for cyclopentane combustion shift to lower temperatures with increasing Pt particle size, from catalyst A-I to catalyst A-III. The CH_4 combustion on Pt occurs at temperatures significantly higher as compared with cyclopentane combustion; on catalyst A-I, the reaction starts at about 713 K and reaches total conversion between 803 and 843 K. In contrast with cyclopentane combustion, the light-off curves for methane oxidation shift to higher temperatures with increasing Pt particle size. Qualitatively, a simi-

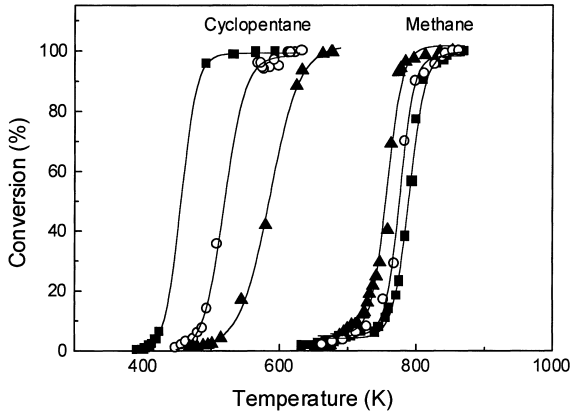

Fig. 1. Light-off curves for cyclopentane and methane combustions. (▲) catalyst A-I; (○) catalyst A-II; (■) catalyst A-III. Cyclopentane combustion: $W/F^0_{CP} = 54$ g catalyst h/mol cyclopentane, $P = 1$ atm, CP:O_2:N_2 = 0.65:10:90. Methane combustion: $W/F^0_{CH_4} = 20$ g catalyst h/mol methane, $P = 1$ atm, CH_4:O_2:N_2 = 2:9.8:88.2.

lar shift of the light-off curves with $\bar{d}_{Pt}$ was observed on unchlorided Pt catalysts (catalysts B-I and B-II).

The effect of the Pt dispersion on catalyst activation was studied by performing two consecutive light-off curves over all the catalysts. At the end of the first catalytic run, the reaction was maintained at 673 K (cyclopentane) or 913 K (methane) for 2 h and then samples were purged and cooled down in nitrogen to 373 K. Subsequently, a second catalytic test was carried out. Fig. 2 shows the X vs. T curves obtained for both reactions on catalysts A-I and A-III in two consecutive catalytic tests. In the case of cyclopentane combustion on catalyst A-I, Fig. 2a shows that the X vs. T curve corresponding to the second run was clearly shifted to lower temperatures as compared to that obtained in the first run. Such a displacement of the light-off curves typically illustrates the catalyst activation phenomenon in hydrocarbon combustion reactions. To compare catalyst activities, we measured from light-off curves the value of the temperature at $X = 50\%$, $T^{50}_{i,j}$, where i identifies the catalyst and j indicates first (1) or second (2) runs. The difference $\Delta T^{50}_i = T^{50}_{i,1} - T^{50}_{i,2}$ is a measure of the activation phenomenon on catalyst i. The $T^{50}_{\text{A-I},j}$ values for cyclopentane combustion are shown in Table 2. It is observed that $T^{50}_{\text{A-I},2}$ was about 85 K lower than $T^{50}_{\text{A-I},1}$. On the other hand, we measured the Pt dispersion on catalyst A-I after the second run (D_2, Table 2). The metallic dispersion on the fresh catalyst ($D_0 = 65\%$) diminished drastically to 20% after the second run.

Fig. 2b shows the consecutive light-off curves obtained for cyclopentane combustion on catalyst A-III; similar experiments were carried out on catalysts A-II, B-I and B-II (not shown here). From consecutive light-off curves we measured $\Delta T^{50}_{\text{A-II}} = 41$ K and $\Delta T^{50}_{\text{A-III}} \cong 0$ K (Table 2). This later result shows that the activation phenomenon is not verified on catalyst A-III. The metallic fraction of fresh catalyst A-II appeared to be severely sintered after two consecutive catalytic tests; the Pt dispersion diminished, in fact, from $D_0 = 38\%$ to $D_2 = 15\%$. On catalyst A-III, the values of D_0 and D_2 were similar, i.e. about 15%. For

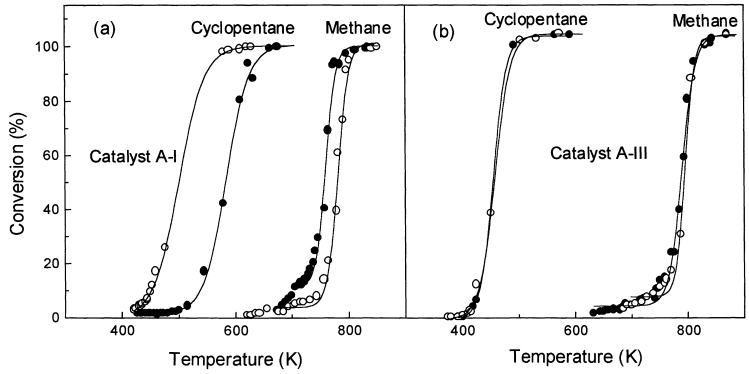

Fig. 2. Consecutive light-off curves: (●) first run; (○) second run. Cyclopentane combustion: $W/F^0_{CP} = 54$ g catalyst h/mol cyclopentane, $P = 1$ atm, CP:O_2:N_2 = 0.65:10:90. Methane combustion: $W/F^0_{CH_4} = 20$ g catalyst h/mol methane, $P = 1$ atm, CH_4:O_2:N_2 = 2:9.8:88.2.

Table 2
Cyclopentane and methane combustions: catalytic activity and Pt dispersion in two consecutive catalytic runs (cyclopentane combustion: $W/F^0_{CP} = 54$ g catalyst h/mol cyclopentane, $P = 1$ atm, CP:O_2:N_2 = 0.65:10:90; methane oxidation: $W/F^0_{CH_4} = 20$ g catalyst h/mol methane, $P = 1$ atm, CH_4:O_2:N_2 = 2:9.8:88.2)

Catalyst	D_0[a] (%)	Cyclopentane combustion				Methane combustion			
		Temperatures at $X = 50\%$ (K)			D_2[b] (%)	Temperatures at $X = 50\%$ (K)			D_2[b] (%)
		T_1^{50}	T_2^{50}	ΔT^{50}		T_1^{50}	T_2^{50}	ΔT^{50}	
A-I	65	585	500	85	20	757	781	−24	15
A-II	38	520	479	41	15	778	791	−13	11
A-III	15	463	463	0	14	793	795	−2	10
B-I	55	562	518	44	25	770	795	−25	9
B-II	19	492	487	5	17	845	848	−3	7

[a] Pt dispersion of fresh catalysts.
[b] Pt dispersion measured after the second catalytic run.

unchlorided catalysts, we determined $\Delta T^{50}_{B\text{-}I} = 44$ K and $\Delta T^{50}_{B\text{-}II} \cong 5$ K.

Regarding methane combustion, Fig. 2a shows that on catalyst A-I the X vs. T curve corresponding to the second run was shifted to higher temperatures as compared to that obtained in the first run; $T^{50}_{A\text{-}I,2}$ was about 24 K higher than $T^{50}_{A\text{-}I,1}$ (Table 2). After two consecutive catalytic tests, the Pt dispersion of catalyst A-I diminished from $D_0 = 65\%$ to $D_2 = 15\%$. Two consecutive methane oxidation tests were also performed on catalysts A-III (Fig. 2b), A-II, B-I and B-II; the obtained $T^{50}_{i,j}$ and ΔT^{50}_i values are given in Table 2. Over chlorided Pt catalysts we measured $\Delta T^{50}_{A\text{-}II} = -13$ K and $\Delta T^{50}_{A\text{-}III} \cong -2$ K. The Pt dispersion of catalyst A-II diminished from $D_0 = 38\%$ to $D_2 = 11\%$, whereas on catalyst A-III the values of D_0 and D_2 were 15 and 10%, respectively. For unchlorided catalysts, we determined $\Delta T^{50}_{B\text{-}I} = -25$ K and $\Delta T^{50}_{B\text{-}II} \cong -3$ K. All these results show that Pt catalysts are not activated ab initio of the methane oxidation reaction. On the contrary, the activity diminishes after a first catalytic test and the light-off curve shifts to higher temperatures. The temperature shift between two consecutive catalytic tests decreases with decreasing Pt particle size and becomes negligible for sintered catalysts A-III and B-II.

3.2. Catalytic tests: kinetic studies

Cyclopentane and methane oxidations were also carried out on platinum catalysts at constant temperatures, between 453 and 523 K (cyclopentane) and between 683 and 733 K (methane). In all the cases, the initial conversion was lower than 10%. Fig. 3 shows the X vs. time curves obtained on catalysts A-I and A-III at 513 K (cyclopentane) and 713 K (methane), and typically illustrates the time on stream behavior of the catalysts during the reactions. For cyclopentane oxidation, the activity of catalyst A-I slowly increases with time along the 8 h runs while on catalyst A-III the cyclopentane conversion remains approximately constant. In the case of methane oxidation, the activity decreases along the run on catalyst A-I but does not change with time on catalyst A-III. Similar catalytic tests were performed on

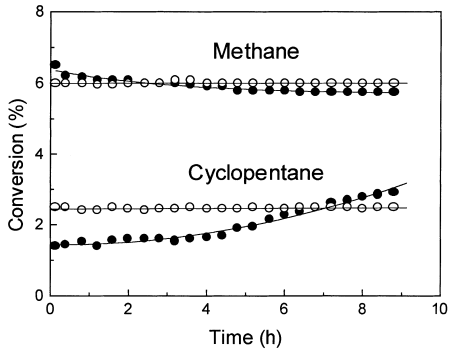

Fig. 3. Methane and cyclopentane conversions as a function of time: (●) catalyst A-I: (○) catalyst A-III. Cyclopentane oxidation: $T = 513$ K, $P = 1$ atm, CP:O_2:N_2 = 0.65:10:90, W/F^0_{CP} was 54 g catalyst h/mol cyclopentane for catalyst A-I and 1.34 g catalyst h/mol cyclopentane for catalyst A-III. Methane oxidation: $T = 713$ K, $P = 1$ atm, CH_4:O_2:N_2 = 2:9.8:88.2; $W/F^0_{CH_4} = 16$ g catalyst h/mol methane.

Table 3
Cyclopentane and methane oxidation rates measured from low-conversion catalytic tests (cyclopentane oxidation: $T = 443\,K$, $P = 1\,atm$, $CP:O_2:N_2 = 0.65:10:90$, $W/F^0_{CP} = 54\,g\,catalyst\,h/mol$ cyclopentane; methane oxidation: $T = 713\,K$, $P = 1\,atm$, $CH_4:O_2:N_2 = 2:9.8:88.2$, $W/F^0_{CH_4} = 12\,g\,catalyst\,h/mol$ methane)

Catalyst	D_0[a] (%)	Cyclopentane combustion			Methane combustion		
		r_0[b] (mol CP/h g Pt)	TOF[c] (h^{-1})	D_f[d] (%)	r_0 (mol CH_4/h g Pt)	TOF (h^{-1})	D_f (%)
A-I	65	0.12	35	42	1.63	490	45
A-II	38	0.60	310	30	1.52	780	35
A-III	15	0.92	1200	14	1.20	1560	15
B-I	55	0.14	50	45	1.55	550	40
B-II	19	0.93	950	18	1.02	1050	18

[a] Pt dispersion of fresh catalysts.
[b] Initial reaction rates.
[c] Initial turnover frequencies.
[d] Pt dispersion measured after the 8 hours catalytic tests.

catalysts A-II, B-I and B-II. The results obtained using unchlorided catalysts confirmed that on well dispersed catalysts (catalyst B-I) the activity increases (cyclopentane) or decreases (methane) with time on stream, whereas on sintered catalysts (catalyst B-II) the hydrocarbon conversion does not change during the runs. To compare intrinsic catalyst activities, we calculated from the X vs. time curves the initial reaction rates (r_0, mol hydrocarbon/h g Pt) and turnover frequencies (TOF per hour) at 443 K (cyclopentane) and 713 K (methane); the values are shown in Table 3. Cyclopentane oxidation turnover rates increased drastically with increasing $\bar{d}_{Pt}$, irrespective of the chlorine level on the samples; the TOF value on catalyst A-III ($D_0 = 15\%$) was about 35 times higher than that measured on catalyst A-I ($D_0 = 65\%$). In contrast, for methane combustion the turnover rate increased slightly with $\bar{d}_{Pt}$; the TOF value measured on catalyst A-III was only three times higher as compared to that on catalyst A-I. After the X vs. time catalytic tests, the metallic dispersion of the samples were measured by hydrogen chemisorption; the obtained values are given in Table 3. For both reactions it is observed that, excepting on sintered catalysts A-III and B-II, the metallic dispersion diminished during the 8 h runs.

The reaction orders on catalysts A-I and A-III were determined by considering for initial reaction rate r_0 a power-law rate equation

$$r_0 = k(P^0_{HC})^{\alpha}(P^0_{O_2})^{\beta}$$

where P^0_k is the partial pressure of reactant k in the feed, and HC represents either cyclopentane or methane. For cyclopentane oxidation the α values were measured by varying the cyclopentane partial pressure between 1.5×10^{-3} and 7.7×10^{-3} atm at a fixed oxygen pressure (0.126 atm). Similarly, reaction order β was obtained by varying $P^0_{O_2}$ between 0.074 and 0.183 atm while keeping P^0_{CP} at 6.5×10^{-3} atm. For methane combustion, the effect of reactant partial pressures on kinetic behavior was study by first measuring catalytic activities at methane partial pressures between 8.2×10^{-3} and 30×10^{-3} atm while $P^0_{O_2}$ was kept constant at 0.126 atm, then measuring at O_2 partial pressures between 0.074 and 0.183 atm while $P^0_{CH_4}$ was kept constant at 0.02 atm. In Figs. 4 and 5, the r_0 values obtained on catalysts A-I and A-III were represented in logarithmic plots as a function of P^0_{HC} and $P^0_{O_2}$, respectively. Reaction orders α and β were determined graphically from Figs. 4 and 5. On both catalysts, we measured $\alpha \cong 0$ and $\beta \cong 1$ for cyclopentane combustion while the reaction orders for methane combustion were $\alpha \cong 1$ and $\beta \cong 0$. In Figs. 6 and 7 we plotted the ln TOF values as a function of $1/T$ for calculating the apparent activation energy (E_a) and the pre-exponential factor A of the hydrocarbon combustion on catalysts A-I and A-III via an Arrhenius-type function. From the slope of the resulting linear plots we obtained E_a values of 11 ± 1 kcal/mol (cyclopentane) and 18 ± 1 kcal/mol (CH_4), irrespective of the mean Pt crystallite size of the sample. For cyclopentane combustion, we measured a $A_{A\text{-III}}/A_{A\text{-I}}$ ratio of about 45.

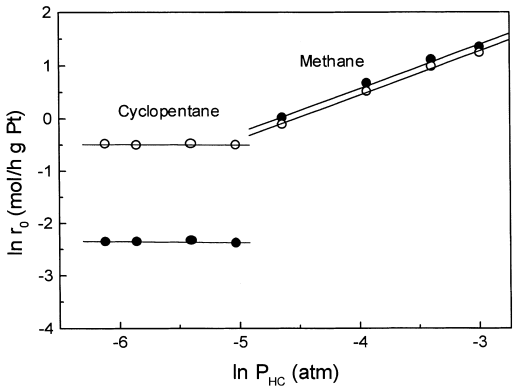

Fig. 4. Dependence of cyclopentane and methane oxidation reactions upon the hydrocarbon partial pressure. (●) catalyst A-I; (○) catalyst A-III. Cyclopentane oxidation: $T = 443\,\mathrm{K}$, $P = 1\,\mathrm{atm}$, $P^0_{O_2} = 0.126\,\mathrm{atm}$. Methane oxidation: $T = 713\,\mathrm{K}$, $P = 1\,\mathrm{atm}$, $P^0_{O_2} = 0.126\,\mathrm{atm}$.

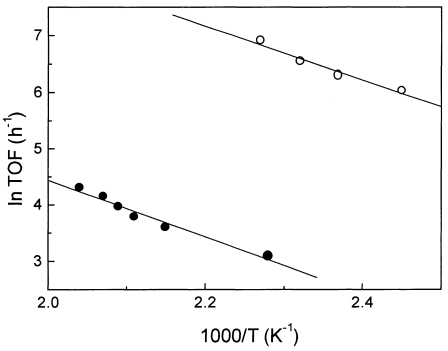

Fig. 6. Arrhenius plots for determining E_a (apparent activation energy) and A (pre-exponential factor). Cyclopentane oxidation turnover rates as a function of inverse temperature on catalysts A-I (●) and A-III (○). $P = 1\,\mathrm{atm}$, $\mathrm{CP{:}O_2{:}N_2} = 0.65{:}10{:}90$, $W/F^0_{CP} = 54\,\mathrm{g\,catalyst\,h/mol}$ cyclopentane.

4. Discussion

4.1. Cyclopentane combustion

For cyclopentane combustion the light-off curves are shifted to lower temperatures with increasing Pt particle size (Fig. 1 and Table 1). The T_1^{50} values diminished on chlorided catalysts from 585 K (catalyst I-A, $D_0 = 65\%$) to 454 K (catalyst A-III, $D_0 = 15\%$), and from 562 K (catalyst B-I, $D_0 = 55\%$) to 492 K (catalyst B-II, $D_0 = 19\%$) on unchlorided catalysts. Results obtained from low-conversion catalytic tests confirmed the effect of Pt particle size on cyclopentane combustion activity. Data in Table 3 show that on all the catalysts cyclopentane oxidation turnover rates drastically increase with increasing $\bar{d}_{Pt}$. Thus, cyclopentane combustion on Pt/Al_2O_3 catalysts is a structure-sensitive reaction preferentially promoted on larger Pt crystallites, irrespective of the chlorine level on the sample.

Reaction orders and the apparent activation energy do not change significantly with changing the metallic dispersion (Figs. 4–6). The higher activity per surface

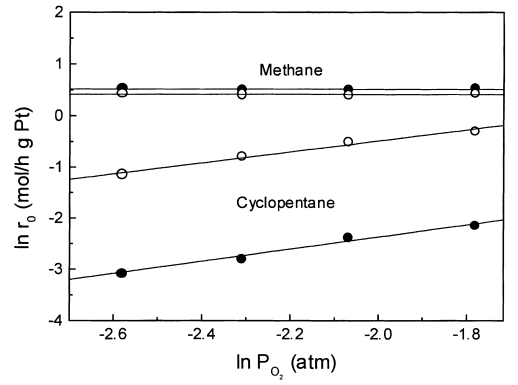

Fig. 5. Dependence of cyclopentane and methane oxidation reactions upon oxygen partial pressure. (●) catalyst A-I; (○) catalyst A-III. Cyclopentane oxidation: $T = 443\,\mathrm{K}$, $P = 1\,\mathrm{atm}$, $P^0_{CP} = P$, cyclopentane $= 6.5 \times 10^{-3}\,\mathrm{atm}$. Methane oxidation: $T = 713\,\mathrm{K}$, $P = 1\,\mathrm{atm}$, $P^0_{CH_4} = 0.02\,\mathrm{atm}$.

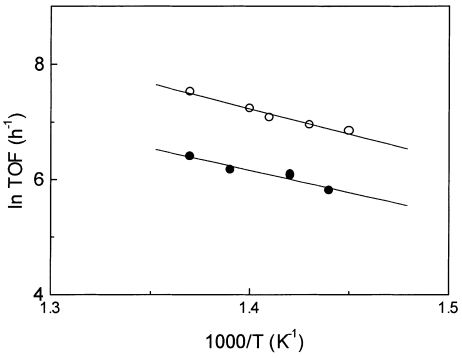

Fig. 7. Arrhenius plots for determining E_a and A. Methane oxidation turnover rates as a function of inverse temperature on catalysts A-I (●) and A-III (○). $P = 1\,\mathrm{atm}$, $\mathrm{CH_4{:}O_2{:}N_2} = 2{:}9.8{:}88.2$, $W/F^0_{CH_4} = 20\,\mathrm{g\,catalyst\,h/mol}$ methane.

Pt atom on low-dispersed Pt catalysts is not caused, therefore, by a change in the combustion reaction mechanism. In contrast, the pre-exponential factor A measured on catalyst A-III was clearly higher than that obtained on catalyst A-I thereby suggesting that the density of active sites changes with increasing Pt particle size.

Our kinetic results may be interpreted by considering that cyclopentane oxidation occurs via a Mars–van Krevelen [24] mechanism. The Mars–van Krevelen mechanism is an oxidative–reductive or "surface redox" mechanism which has been widely used for the oxidation of organic compounds [25,26]. For cyclopentane oxidation on Pt, this mechanism may be represented by the following elementary steps:

$$\tfrac{1}{2}O_2 + Pt^0 \xrightarrow{k_1} O \cdot Pt \quad (1)$$

$$CP + O \cdot Pt \xrightarrow{k_2} [\text{intermediate products}] \xrightarrow{O.Pt} CO_2 + H_2O + Pt^0 \quad (2)$$

By considering the above steps to be first orders in the respective reactants the expression of initial rate r_0 results [27]:

$$r_0 = \frac{k_1 P^0_{O_2} P^0_{CP}}{(k_1/k_2) P^0_{O_2} + \nu_i P^0_{CP}} \quad (3)$$

where ν_i is the stoichiometric coefficient of oxygen in the overall reaction. If $k_1 \ll k_2$ Eq. (3) reduces to

$$r_0 = \frac{k_1 P^0_{O_2}}{\nu_i} \quad (4)$$

and the orders with respect to cyclopentane and oxygen predicted by Eq. (4) are 0 and 1, respectively, which are the approximate orders determined from our experiments. An apparent zeroth-order reaction with respect to the hydrocarbon has been previously reported for the oxidation of different aromatic hydrocarbons (namely benzene, toluene, *o*-xylene, ethylbenzene) over platinum-based catalysts [2,27,28]. In contrast, an apparent first-order reaction in oxygen has been observed only with benzene [29]. For cyclopentane combustion, Eq. (4) is the limiting form of Eq. (3) and is obtained when the dissociative adsorption of oxygen on platinum is rate-determining in the surface redox mechanism represented by reactions (1) and (2). Any increase in rate constant k_1 accelerates in this case the cyclopentane oxidation rate. Our results show that by diminishing the Pt dispersion, the apparent activation energy for cyclopentane oxidation reaction does not change but the pre-exponential factor A clearly increases. The observed turnover rate increase with increasing Pt particle size would reflect therefore an increase in the density of reactive Pt–O species resulting from higher Pt oxidation rates. Duprez [30] studied the effect of the particle size on the adsorption/desorption rate of oxygen on Rh, Pd and Pt by $^{18}O_2$ isotopic exchange techniques. He found that the $^{18}O_2 + {}^{16}O_2$ equilibration turnover rate increases more than two orders when the Pt dispersion is decreased from 57 to 4%. Briot et al. [7] reported that on larger Pt crystallites the heat of oxygen chemisorption decreases and the reactivity of chemisorbed oxygen increases. The lower reactivity of very small oxidized Pt particles toward hydrogen was observed by several authors [31,32]. In well-dispersed platinum-supported catalysts, platinum is completely oxidized to PtO_2 when treated in oxygen at temperatures higher than 473 K [33]. However, McCabe et al. [32] reported that only the surface of large Pt crystallites is oxidized during heating in air up to 873 K. In recent studies using X-ray absorption spectroscopy (EXAFS) we investigated the Pt–O interaction on fresh and sintered Pt/Al_2O_3 catalysts following the sample oxidation in oxygen at 573 K [34]. We found that on sintered catalysts the Pt–Pt coordination increases while the Pt–O coordination decreases as compared with fresh catalysts. The structural information supplied by EXAFS showed that the oxidation of large Pt crystallites involves only the outermost metal shell. Based on similar evidences, Hicks et al. [4] considered that by increasing the Pt particle size the interaction of oxygen with platinum goes from a "surface oxide" to a "chemisorbed layer" oxygen species. All these results are consistent with the assumption that the number of Pt–O bonds of lower binding energy, i.e. the site density of more reactive surface oxygen, increases on larger Pt particles.

Fig. 2 and Table 2 show that on chlorided Pt/Al_2O_3 catalysts of high metallic dispersion (catalysts A-I and A-II) the light-off curves are shifted to lower temperatures after a first catalytic test. Unchlorided catalyst B-I exhibited a similar qualitative shift of the consecutive light-off curves (Table 2), thereby suggesting that the observed catalyst activation

phenomenon is not caused by the presence of chlorine on the support. Marceau et al. [21] reported that the hydrocarbon oxidation activity on chlorided Pt/Al_2O_3 catalysts increases with time concomitantly with chlorine elimination from the support. Based in previous work showing that chlorine may block the active sites for alkane oxidation on Pd [35] and Pt [15], these authors concluded that the elimination of chlorine on stream increases the accessibility of reactant gases to metallic Pt sites and as a result the activity increases. However, our results show that the initial activation phenomenon takes place on well-dispersed platinum catalysts irrespective of the chlorine level on the catalysts. In a recent study on the oxidation of benzene over Pt/Al_2O_3 we showed that activating induction periods are not related to the in situ formation of oxidized or oxychlorided Pt^{n+} species [14]. As already stated by others, platinum remains in zero valence state throughout catalytic oxidation of hydrocarbons [20].

The metallic fraction of well-dispersed chlorided and unchlorided Pt/Al_2O_3 catalysts appeared severely sintered after two consecutive X vs. T tests. The Pt dispersion of catalyst A-I dropped from 65 to 20%, and that of catalyst B-I, from 55 to 25% (Table 2). In contrast, on low-dispersed Pt catalysts the consecutive light-off curves are similar and the metallic dispersion is not significantly modified (results for catalyst A-III and B-II in Fig. 2b and Table 2). The dependence of the activation phenomenon with the platinum dispersion is confirmed by the results obtained from low-conversion catalytic tests. Fig. 3 shows that while cyclopentane conversion increases with time on well-dispersed catalyst A-I, the activity of sintered catalyst A-III does not change on stream. On the other hand, hydrogen chemisorption measurements (Table 3) show that the increase of the cyclopentane conversion with time on catalysts A-I, A-II and B-I parallels a concomitant increase in the Pt particle size. The general picture emerging from the above results is that the initial activation of well-dispersed Pt catalysts is caused by the sintering of the metallic phase, which occurs on stream even if the reaction is performed at low-temperature and low-conversion regimes. Cyclopentane oxidation is highly exothermic ($-\Delta H = 752\,\text{kcal/mol}$) and the Pt crystallite temperature is significantly increased during reaction. Hot-spots on the metallic particles together with the presence of gaseous water cause the metal phase sintering and the formation of larger, more active, Pt particles. As a result, the cyclopentane conversion increases with time until the formation of larger steady state Pt particles is completed.

4.2. Methane combustion

The catalytic conversion of methane has been proven to be significantly harder than any other hydrocarbon [25,36]: light-off temperatures 200–300 K higher than that of cyclopentane combustion are observed in Fig. 1. In contrast with cyclopentane combustion, the light-off curves for methane combustion are shifted to higher temperatures with increasing Pt particle size (Fig. 1). Table 2 shows that T_1^{50} values increase on chlorided catalysts from 757 K (catalyst A-I, $D_0 = 65\%$) to 793 K (catalyst A-III, $D_0 = 15\%$), and from 770 K (catalyst B-I, $D_0 = 55\%$) to 845 K (catalyst B-II, $D_0 = 19\%$) on unchlorided catalysts. These results are in line with data obtained from low-conversion catalytic tests which show that methane oxidation rate r_0 (mol CH_4/h g Pt) diminishes when the Pt dispersion is decreased (Table 3). However, the turnover frequency increases with increasing $\bar{d}_{Pt}$ by a factor of about 3 in the Pt dispersion range investigated (Table 3), thereby indicating that the activity per surface Pt atom is higher on larger Pt crystallites. Previous reports agree in that methane oxidation on Pt-based catalysts is promoted on larger Pt crystallites [4,37]. Hicks et al. [4] found that the methane oxidation turnover rate at 608 K increases on supported platinum from $18\,h^{-1}$ (dispersed phase of Pt) to $290\,h^{-1}$ (crystalline phase of Pt). Our results show only a moderate increase of the TOF value with $\bar{d}_{Pt}$ that does not compensate the activity loss caused by the simultaneous diminution of the number of surface Pt atoms. As a consequence, r_0 diminishes with increasing $\bar{d}_{Pt}$ and the light-off curves shift to higher temperatures.

Kinetic studies show that methane oxidation on Pt/Al_2O_3 is order one in methane and order zero in oxygen (Figs. 4 and 5), in agreement with previous studies [37,38]. Reaction orders and the apparent activation energy do not change with changing the metallic dispersion (Figs. 4, 5 and 7), thereby suggesting that the methane oxidation mechanism is the same on well-dispersed and sintered catalysts. The methane oxidation rate law has been interpreted to be the consequence of an initial slow activation step for the

hydrocarbon on an oxygen-covered surface [37,39]. In particular, a good correlation was observed between C–H bond energies and reactivities, suggesting that the initial activation of the alkane is the rate-limiting step for the overall combustion process [20,35]. We interpret the methane oxidation mechanism in terms of Mars–van Kravelen reduction–oxidation pathways, where the rate-determining step is the abstraction of the first hydrogen on the adsorbed methane molecule and oxygen chemisorption steps are not kinetically significants [19]. The proposed reaction pathways:

$$2O_2 + 4 \cdot L \overset{K_1}{\leftrightarrow} 4O \cdot L$$

$$CH_4 + L \overset{K_2}{\leftrightarrow} CH_4 \cdot L$$

$$CH_4 \cdot L + O \cdot L \overset{k}{\rightarrow} CH_3 \cdot L + OH \cdot L$$

$$CH_3 \cdot L + 3O \cdot L \overset{K_3}{\leftrightarrow} C \cdot L + 3OH \cdot L$$

$$C \cdot L + 2O \cdot L \overset{K_4}{\leftrightarrow} CO_2 \cdot L + 2L$$

$$4OH \cdot L \overset{K_5}{\leftrightarrow} 2H_2O_{(g)} + 2O \cdot L + 2L$$

$$CO_2 \cdot L \overset{K_6}{\leftrightarrow} CO_{2(g)} + L$$

lead to a complex kinetic rate expression

$$r = \frac{kK_3\sqrt{K_1K_2}P_{CH_4}[P_{O_2}]^{1/2}}{\left[1 + K_3P_{CH_4} + \sqrt{K_1K_2}[P_{O_2}]^{1/2} + K_1P_{O_2} + \sqrt{\frac{(K_1K_2)^{1/2}}{K_5}}[P_{H_2O}]^{1/2}[P_{O_2}]^{1/4} + \frac{P_{CO_2}}{K_6} + \frac{\sqrt{K_1K_6}}{K_6}[P_{O_2}]^{1/2}P_{CO_2}\right]^2}$$

When hydroxyl groups are the most abundant species, the initial rate expression becomes

$$r_0 = \frac{kK_3K_5P^0_{CH_4}}{P^0_{H_2O}} \quad (5)$$

Eq. (5) predicts orders zero and one in O_2 and methane, respectively, in agreement with the observed experimental rate equation. Eq. (5) also predicts a negative order -1 with respect to water.

In contrast with the results obtained for cyclopentane combustion, we do not observe the existence of initial activation periods for methane oxidation on chlorided or unchlorided Pt/Al_2O_3 catalysts (Figs. 2 and 3, and Table 2). As in the case of cyclopentane combustion, the Pt crystallites of well-dispersed catalysts growth on stream forming larger particles ab initio of the methane oxidation reaction, but the activity does not increase (Fig. 3). This different catalytic behavior observed by comparing cyclopentane and methane combustions is explained by considering the dependence of oxidation turnover rates with $\bar{d}_{Pt}$; by increasing $\bar{d}_{Pt}$ 4.3 times, the TOF value increases about two orders of magnitude for cyclopentane but only by a factor of 3 for methane (Table 3). Cyclopentane conversion increases with time on stream because the TOF increase caused by metal sintering largely exceed the activity drop caused by the concomitant diminution of surface Pt concentration. On the contrary, for methane oxidation the loss of active sites by sintering in reaction conditions is higher than the turnover rate increase and, as a consequence, the methane conversion decreases with time. Slow steps in cyclopentane and methane oxidation mechanisms are different, probably reflecting differences in the competitive adsorption of the hydrocarbon and oxygen on the metal surface. The structure sensitivity of hydrocarbon oxidation reactions is related to the structure sensitivity of the rate-limiting step in the oxidation reaction mechanism. On platinum, the TOF increase with $\bar{d}_{Pt}$ for dissociative oxygen adsorption (rate-limiting step for cyclopentane oxidation) would be substantially higher than for the dissociative chemisorption of methane (rate-limiting step for methane oxidation). This difference in the structure sensitivity of the slowest steps on Pt/Al_2O_3 catalysts explains that the initial activation phenomenon is verified on well-dispersed catalysts only for cyclopentane oxidation.

5. Conclusions

Cyclopentane and methane oxidations on Pt/Al_2O_3 proceed via different reaction mechanisms. Cyclopentane is oxidized on metallic Pt active sites via a surface redox mechanism, being the dissociative adsorption of oxygen on platinum the rate-determining step. Increasing the Pt particle size increases drastically the density of reactive Pt–O species available

for the rate-determining step and, as a consequence, the reaction is preferentially promoted on larger Pt crystallites. Cyclopentane oxidation is first order in oxygen and zeroth order in the hydrocarbon, and the reaction mechanism does not change by changing the metallic dispersion. The activity for cyclopentane oxidation on well-dispersed Pt catalysts increases with time on stream, irrespective of the chlorine level on the sample. Activating induction periods during catalytic oxidation of cyclopentane are caused by the in situ sintering of the metallic phase ab initio of the reaction. Steady-state conditions are reached when the rate growth of Pt particles is negligible because of the formation of very large Pt particles.

For methane oxidation, kinetic results are consistent with a reaction mechanism which includes the abstraction of the first hydrogen on the adsorbed methane molecule as the rate-determining step. Methane oxidation is order zero and one with respect to oxygen and methane, respectively, and the turnover rate increases only slightly with increasing Pt particles. On well-dispersed Pt catalysts, the reaction does not exhibit initial activation periods. Methane conversion diminishes with time on stream because the loss of active sites by Pt sintering in reaction conditions is higher than the turnover rate increase on larger metallic crystallites.

Acknowledgements

We acknowledge E. Rincón for his participation in some of the catalytic experiments. We thank the Consejo Nacional de Investigaciones Científicas y Técnicas (CONICET), Argentina, and the Universidad Nacional del Litoral, Santa Fe, Argentina, for financial support.

References

[1] J.J. Spivey, Ind. Eng. Chem. Res. 26 (1987) 2165.
[2] K.T. Chuang, S. Cheng, S. Tong, Ind. Eng. Chem. Res. 31 (1992) 2466.
[3] J. Hermia, S. Vigneron, Catal. Today 17 (1993) 349.
[4] R.F. Hicks, H. Qi, M.L. Young, R.G. Lee, J. Catal. 122 (1990) 280.
[5] F.H. Ribeiro, M. Chow, R.A. Dalla Beta, J. Catal. 146 (1994) 277.
[6] K. Otto, Langmuir 5 (1989) 1364.
[7] P. Briot, A. Auroux, D. Jones, M. Primet, Appl. Catal. 59 (1990) 141.
[8] M. Kobayashi, T. Kanno, A. Konishi, H. Takeda, React. Kinet. Catal. Lett. 37 (1988) 89.
[9] V. Labalme, E. Garbowsky, N. Ghilhaume, M. Primet, Appl. Catal. A 138 (1996) 93.
[10] R.F. Hicks, R.G. Lee, W.J. Han, A.B. Kooh, in: R.K. Graselli, W. Sleight (Eds.), Structure-activity and Selectivity Relationship in Heterogeneous Catalysis, Elsevier, Amsterdam, 1991, p. 127.
[11] C. Pliangos, I.V. Yentekakis, V.G. Papadakis, C.G. Vayenas, X.E. Verykios, Appl. Catal. B 14 (1997) 161.
[12] P. Papaefthimiou, T. Ioannides, X.E. Verykios, Appl. Catal. B 15 (1998) 75.
[13] G. Dalmai-Imelik, C. Leclercq, I. Mutin, J. Micr. Spectr. Elec. 20 (1974) 123.
[14] T.F. Garetto, C.R. Apesteguía, Appl. Catal. B, submitted for publication.
[15] P. Marécot, A. Fakche, B. Kellali, G. Mabilon, M. Prigent, J. Barbier, Appl. Catal. B 3 (1994) 283.
[16] C. Pliangos, I.V. Yentekakis, V.G. Papadakis, C.G. Vayenas, X.E. Verykios, Appl. Catal. B 14 (1997) 161.
[17] P. Papaefthimiou, T. Ioannides, X.E. Verykios, Appl. Catal. B 15 (1998) 75.
[18] R. Burch, P.K. Loader, F.J. Urbano, Catal. Today 27 (1996) 243.
[19] K. Fujimoto, F. Ribeiro, H.M. Avalos Borja, E. Iglesia, J. Catal. 179 (1996) 431.
[20] M. Aryafar, F. Zaera, Catal. Lett. 48 (1997) 173.
[21] E. Marceau, M. Che, J. Saint-Just, J.M. Tatibouët, Catal. Today 29 (1996) 415.
[22] J.M. Sinfelt, J.L. Carter, D.J.C. Yates, J. Catal. 24 (1972) 283.
[23] L. Spenadel, M. Boudart, J. Phys. Chem. 64 (1960) 204.
[24] P. Mars, D.W. van Kravelen, Chem. Eng. Sci. 3 (1954) 41.
[25] G.I. Golodets, Heterogeneous Catalytic Reactions Involving Molecular Oxygen, Studies in Surface Science and Catalysis, Vol. 15, Elsevier, Amsterdam, 1983.
[26] S. Balasubramanian, D.S. Viswanath, Ind. Eng. Chem. Fundam. 14 (1975) 158.
[27] S.K. Gangwal, M.E. Mullins, J.J. Spivey, P.R. Caffrey, Appl. Catal. 36 (1988) 231.
[28] A.A. Barresi, G. Baldi, Chem. Eng. Sci. 47 (1992) 1943.
[29] A.A. Barresi, G. Baldi, Ind. Eng. Chem. Res. 33 (1994) 2964.
[30] D. Duprez, in: Can Li, Qin Xin (Eds.), Studies in Surface Science and Catalysis, Vol. 112, Elsevier Science, 1997, p. 13.
[31] H.C. Yao, M. Sieg, H.K. Plummer, J. Catal. 59 (1979) 365.
[32] R.W. McCabe, C. Wong, H.S. Woo, J. Catal. 144 (1988) 354.
[33] H. Lieske, G. Lietz, H. Spindler, J. Volter, J. Catal. 81 (1983) 8.
[34] A. Borgna, F. Le Normand, T.F. Garetto, C.R. Apesteguía, B. Moraweck, Catal. Lett. 13 (1992) 175.
[35] D.O. Simone, T. Kennelly, N.L. Brungard, R.J. Farrauto, Appl. Catal. 70 (1991) 87.
[36] R. Burch, M.J. Hayes, J. Molec. Catal. A 100 (1995) 13.
[37] Y.F.Y. Yao, Ind. Eng. Chem. Prod. Res. Dev. 5 (1980) 293.
[38] M. Niwa, K. Awano, Y. Murakami, Appl. Catal. 7 (1983) 317.
[39] C.F. Cullis, D.E. Keene, D.L. Trimm, J. Catal. 19 (1970) 864.